



## Research Article

# Heat transfer model for dropwise condensation on hydrophobic and superhydrophobic interfaces

R. YUVARAJ<sup>1,\*</sup> , D. SENTHILKUMAR<sup>1</sup> 

<sup>1</sup>Department of Mechanical Engineering, Sona College of Technology, Salem, Tamilnadu, 636005, India

## ARTICLE INFO

### Article history

Received: 01 April 2022

Revised: 02 August 2022

Accepted: 11 August 2022

### Keywords:

Dropwise Condensation;  
Biot Number; Heat Transfer;  
Hydrophobic Surface;  
Superhydrophobic Surface;  
Interface Temperature

## ABSTRACT

Heat transfer models for condensation on hydrophobic and superhydrophobic interfaces are broadly available based on thermal resistance correlations. In the previous studies, very few models are presented based on the scaling factor or Nusselt number, and no model is available that directly correlates Biot number. This study develops a heat transfer model for dropwise condensation underneath a horizontal surface. The present model correlates with the Biot number to predict the heat transfer, temperature variation at the interfaces, solid-liquid, and liquid-vapor, and the growth rate of droplet condensate on the hydrophobic and superhydrophobic interfaces by using Archimedes' hat-box theorem. The present model is validated with analytical and experimental results against hydrophobic and superhydrophobic contact angles of similar working parameters made excellent agreements. The analytical model for dropwise condensation produces inaccurate results due to discrepancies and discontinuities due to multiple correlations in the modeling. The present model is modified to obtain a continuous result using experimental data. The modified model is used for analyzing heat transfer by varying Biot numbers from 0.0001 to 1000 using Python 3.6.1 with an accuracy of  $10^{-4}$ . Simulation of the present model results in constant heat transfer at  $Bi = 4$ , irrespective of the contact angle. A negligible amount of coating resistance and interface resistance when  $Bi > 0.1$ , curvature effect when  $Bi > 0.04$ , droplet resistance when  $Bi < 0.02$ , the maximum liquid-vapor interface temperature at  $Bi \approx 10$ , and maximum solid-liquid interface temperature at  $Bi \approx 5$ , are presented.

**Cite this article as:** Yuvaraj R, Senthilkumar D. Heat transfer model for dropwise condensation on hydrophobic and superhydrophobic interfaces. J Ther Eng 2023;9(5):1245–1259.

## INTRODUCTION

Condensation is a phase change mechanism widely used in many applications such as power generation [1-3], desalination [4], electronic thermal management [5], heat exchangers [6], building energy management [7-8], refrigeration, and air conditioning system [9]. Condensation on

non-wetting surfaces offers dropwise condensation due to low surface energy. The focus on dropwise condensation has increased widely since its discovery in 1930 [10]. This mechanism yields heat transfer rates up to an order of magnitude higher than filmwise condensation [11-12]. The low surface energy of a substrate offers increases in contact

### \*Corresponding author.

\*E-mail address: [yuvarajr@sonatech.ac.in](mailto:yuvarajr@sonatech.ac.in)

This paper was recommended for publication in revised form by Regional Editor Omid Mahian



angle ( $\theta$ ) from hydrophilic ( $\theta < 90^\circ$ ) to hydrophobic ( $\theta > 90^\circ$ ) surfaces. Several works have since fabricated superhydrophobic ( $\theta \geq 150^\circ$ )  $\theta \geq 150^\circ$  surfaces to achieve a variety of applications, including self-cleaning, defrosting, and condensation heat transfer enhancement. The initial droplet size of a diameter  $< 1 \mu\text{m}$  condensate on the dropwise condensation process at discrete nucleation sites distributed over a cooled surface [13]. The minimum thermodynamically viable radius ( $r_{min}$ ) [14] of the condensed droplet grows due to condensation and coalescence with neighboring droplets until they become large enough ( $r_{max}$ ) to be removed by gravity. The Rolling and merging of large droplets grow up to the maximum diameter and depart from the surface. This allows new primary droplets of radius  $r_{min}$  to form and grow from nucleation sites to the maximum radius  $r_{max}$ .

In dropwise condensation, heat from the vapor transfers through the liquid-vapor interface and then transfers through the droplet by conduction to the cooled wall. Though many experimental studies [15-31] and numerical studies [32-35] of dropwise condensation on hydrophobic and superhydrophobic surfaces have been conducted in the past decades, accurate modeling of the heat transfer process has lagged. Kim and Kim proposed an analytical model to predict the heat transfer rate ( $Q_d$ ) through a single droplet by considering heat drop due to interfacial resistance ( $\Delta T_i$ ), curvature resistance ( $\Delta T_c$ ), droplet resistance ( $\Delta T_{drop}$ ), and the coating resistance ( $\Delta T_{coat}$ ) [36]. Chavan et al. proposed an individual heat transfer model with the Nusselt number  $Nu$  defined as the ratio of convective resistance to conductive resistance and the Biot number  $Bi$  defined as the ratio of internal resistance to surface resistance.

Adhikari et al. presented the average heat flux through the base of the droplet as [35] with the scaling factor  $f(Bi, \theta)$  is a function of Biot number  $Bi$  and contact angle  $\theta$ , for the conduction contribution to the overall thermal resistance. Most of the previous studies' assumed  $f = 0$  for an infinitely conductive droplet [14,39]. Several studies have been performed to determine the formulae for  $f(Bi, \theta)$ . Sadhal and Martin proposed a model to find the scaling factor for contact angle ( $\theta < 90^\circ$ ) [41]. Yuvaraj et al. [42] reported dropwise condensation on the superhydrophobic surface with regular complete sphere-like droplets, increasing the contact surface area between the vapor and the plate surface. There is no room for the formation of films on the superhydrophobic surface. Instead, the water particles are formed as droplets, resulting decrease in resistance to the flow of heat and the fall-off diameter of the droplet from the superhydrophobic surface. This causes an increase in the heat transfer coefficient of dropwise condensation and the rate of condensation. Chavan et al. have reported numerical and experimental results for hydrophobic surfaces ( $\theta > 90^\circ$ ) along with three different correlations to predict  $f(Bi, \theta)$  [21]. Generally, this model would provide discontinuity in the simulation for dropwise condensation analyses. Accurate modeling of the continuous heat transfer process

from nano-size to the macro size of the condensate droplet on hydrophobic and superhydrophobic interfaces is currently unavailable.

In the present study, a simple heat transfer model for dropwise condensation in terms of Biot number is developed to provide continuous results for heat transfer, temperature variation at the interfaces, and the growth rate of droplet condensate on the hydrophobic and superhydrophobic interfaces by using Archimedes' hat-box theorem. The present model is validated with analytical results obtained using the Kim and Kim model [36] and experimental results given by Chavan et al. [21] of similar working parameters made excellent agreements. The continuous results from the nano to the macro level are obtained from the present model and compared with the experimental data presented by Chavan et al. [21]. The modified model is used for analyzing heat transfer, heat flux, the growth rate of the droplet, and heat drops due to various thermal resistances and interface temperatures by varying Biot numbers  $Bi = 0.001 \rightarrow 1000$  using Python 3.6.1 with an accuracy of  $10^{-4}$ . Python is an open-source high-level computer language and very simple compared to other high-level languages. The present dropwise condensation heat transfer model is developed and executed by creating code using Python version 3.6.1. Python contains many libraries, including NumPy, Matplotlib, Xlsxwriter, etc., for solving linear algebraic equations, plotting the results, and storing the data. Python 3.6.1 version also supports the plotting of contours and heat maps.

## MODELING APPROACH

The analytical heat transfer model presented by Kim and Kim is given as [36]

$$\Delta T_i = \frac{Q_d}{h_i 2\pi r^2 (1 - \cos\theta)} \quad (1)$$

$$\Delta T_c = \frac{r_{min}}{r} \Delta T \quad (2)$$

$$\Delta T_{drop} = \frac{Q_d \theta}{4\pi r k \sin\theta} \quad (3)$$

$$\Delta T_{coat} = \frac{Q_d \delta}{\pi r^2 k_{coat} \sin^2 \theta} \quad (4)$$

$$Q_{d\text{ Kim}} = \frac{\Delta T \pi r^2 \left(1 - \frac{r_{min}}{r}\right)}{\left(\frac{\delta}{k_{coat} \sin^2 \theta} + \frac{r\theta}{4k \sin\theta} + \frac{1}{2h_i(1 - \cos\theta)}\right)} \quad (5)$$

where  $h_i$  is the interfacial heat transfer coefficient,  $r$  is the radius of the droplet,  $\theta$  is the contact angle,  $k$  is the thermal conductivity of the water droplet,  $\delta$  is promoter coating layer thickness,  $k_{coat}$  is the thermal conductivity of the coating, and  $r_{min}$  is the minimum thermodynamic viable radius of the droplet. The heat transfer through a droplet also be calculated from the enthalpy dissipated by the condensing vapor [34]

$$Q_d = \rho h_{fg} \pi r^2 (1 - \cos\theta)^2 (2 + \cos\theta) \frac{dr}{dt} \quad (6)$$

where  $\rho$  is the density of water,  $h_{fg}$  is the latent heat and  $\frac{dr}{dt}$  is the growth rate of droplet condensate. The interfacial heat transfer coefficient is determined by using the kinetic theory [37-38].

$$h_i = \frac{2\alpha}{2 - \alpha} \frac{1}{\sqrt{2\pi R_g T_{sat}}} \frac{h_{fg}^2}{v_g T_{sat}} \quad (7)$$

where  $\alpha$  is the condensation coefficient,  $R_g$  is the gas constant,  $v_g$  is the specific volume of vapor and  $T_{sat}$  is the saturation temperature of the vapor. Condensation coefficient  $\alpha$  is defined as the ratio of vapor molecules captured by the liquid phase to the total number of vapor molecules reaching the liquid surface ( $\alpha = 0 \rightarrow 1$ ). In the present work, a clean environment is assumed, and  $\alpha$  is taken as 1.

Chavan et al. proposed an individual heat transfer model as [21]

$$Q_{d \text{ Chavan}} = \frac{\Delta T \pi r^2 \left(1 - \frac{r_{min}}{r}\right)}{\left(\frac{\delta}{k_{coat} \sin^2 \theta} + \frac{\pi r}{Nu(Bi, \theta) k \sin \theta}\right)} \quad (8)$$

where  $Nu$  is the Nusselt number defined as the ratio of convective resistance to conductive resistance, and  $Bi$  is the

Biot number defined as the ratio of internal resistance to surface resistance. Adhikari et al. presented the average heat flux through the base of the droplet as [35]

$$q = \frac{\Delta T}{\left(\frac{f(Bi, \theta)r}{k} + \frac{1}{2h_i}\right)} \quad (9)$$

where,  $f(Bi, \theta)$  is the scaling factor, a function of Biot number  $Bi$  and contact angle  $\theta$ , for the conduction contribution to the overall thermal resistance. Most of the previous studies' assumed  $f = 0$  for an infinitely conductive droplet [14,39]. For  $f = 0.25$  as assumed by Graham and Griffith [40], the conduction-front propagation velocity ( $\frac{\alpha}{r} = 1.6 \times 10^{-4}$ )  $m/s$  is greater than the growth velocity ( $\frac{dr}{dt} = 6 \times 10^{-7}$ )  $m/s$ . Several studies have been performed to determine the formulae for  $f(Bi, \theta)$ .

Figure 1 shows the water droplet underneath a flat surface of radius  $r$ , contact radius  $r_c$ , droplet height  $h$ , contact angle  $\theta$  with negligible hysteresis, equivalent height  $H$ , the volume of the droplet  $V$ , and its equivalent volume  $V_e$  is obtained from Archimedes' hat-box theorem [43]. By equating  $V = V_e$ , the relation between  $h$  and  $H$  can be written as

$$H = \frac{2h}{3 \sin^2 \theta} \quad (10)$$

Rose and Glicksman reported that most heat is transferred through tiny droplets of constant condensation rate with time [46]. Droplet diameter  $d < 150 \mu m$  transfer 90% of total heat for low-pressure condensation, which occupies 35% of surface area, and  $d < 40 \mu m$  transfer 90% of heat at atmospheric pressure with 23% of the surface area [40]. Droplets in this size range are sufficiently small such that Marangoni circulation and other convection effects can be neglected [45-46]. Hence, conduction is the primary

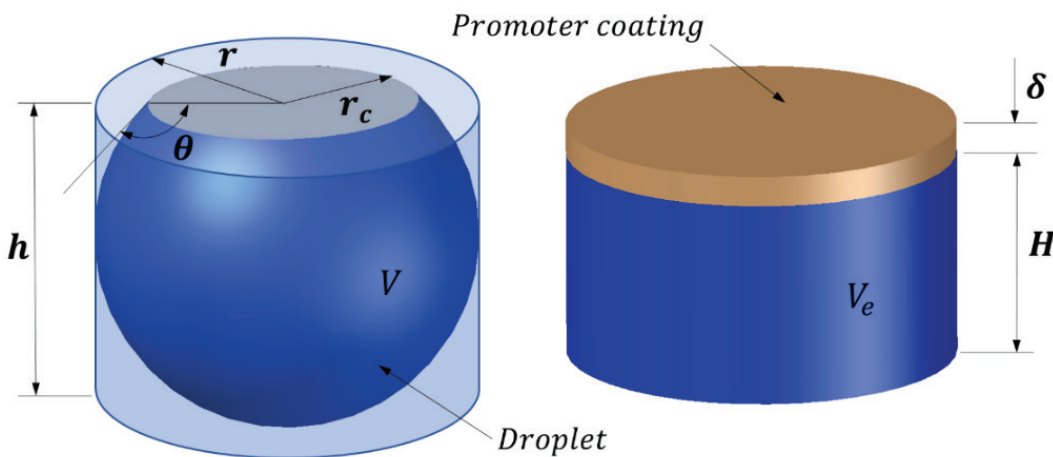


Figure 1. Droplet and its equivalent volume.

mode of heat transfer in dropwise condensation. As droplets grow, the internal temperature distribution varies, and conduction-front propagation velocity is much greater than the droplet growth rate. Therefore, the heat transfer process can be modeled as quasi-steady, and the in-droplet condensation heat transfer process reduces to conduction in a solid medium [35]. With this assumption, the conductive resistance of the droplet can be rewritten as

$$\Delta T_{drop} = \frac{Q_d H}{\pi r^2 k} \quad (11)$$

The Biot number  $Bi$  and the Nusselt number  $Nu$  are defined in terms of contact radius  $r_c$  as

$$Bi = \frac{h_i r_c}{k} \quad (12)$$

$$Nu = \frac{Q_d}{k r_c (T_{sat} - T_s)} \quad (13)$$

After substituting and rearranging the eq (10) and eq (11) in eq (5), the heat transfer model in terms of Biot number can be expressed as

$$Q_d = \frac{c Bi^2 \Delta T \left(1 - \frac{r_{min}}{r}\right)}{\left(a + b Bi + \cos\theta + \frac{2}{3} Bi(1 - \cos\theta)\right)} \quad (14)$$

where  $c = 6\pi k^2/h_i$  is the condensation coefficient,  $a$  is the empirical value and  $b = Bi_{coat}/Bi$  is the Biot number ratio between a coating to the droplet. The following parameters are assumed as similar to the previous works [34–36], interface heat transfer coefficient  $h_i = 400 \text{ MW/m}^2 \text{ K}$ , the thermal conductivity of the water droplet  $k = 0.6 \text{ W/mK}$ , the thermal conductivity of the coating layer  $k_c = 0.2 \text{ W/mK}$ , coating thickness  $\delta = 1 \mu\text{m}$ , the minimum radius  $r_{min} \approx 10 \text{ nm}$ , Subcooling temperature  $\Delta T = 10 \text{ K}$ , the density of the liquid  $\rho = 998 \text{ kg/m}^3$ , latent heat of condensation  $h_{fg} = 2.3 \text{ MJ/kg}$ , and the saturation temperature  $T_{sat} = 373.15 \text{ K}$ .

The Biot number for coating is obtained as  $Bi_{coat} = 2$  from the parameters mentioned above. The value of  $a$  is obtained from the experimental values given by Chavan et al. After substituting the values of  $a$  and  $b$  in eq (14) further, the equation reduced to

$$Q_d = \frac{c Bi^2 \Delta T \left(1 - \frac{r_{min}}{r}\right)}{\left(13 + \cos\theta + \frac{2}{3} Bi(1 - \cos\theta)\right)} \quad (15)$$

Eq (15) is the modified heat transfer model used in the present work without noncondensable gases during condensation. The present model can simulate heat transfer

through the droplet, predict interface temperatures, heat drop due to various resistances, and growth rate of condensate on hydrophobic and superhydrophobic interfaces for varying Biot numbers ( $Bi = 0.0001 \rightarrow 1000$ ).

$$\frac{dr}{dt} = \frac{Q_d}{\rho h_{fg} \pi r^2 (1 - \cos\theta)^2 (2 + \cos\theta)} \quad (16)$$

Eq (16) is used to find the growth rate of condensate on hydrophobic and superhydrophobic interfaces for varying Biot numbers ( $Bi = 0.0001 \rightarrow 1000$ ) [34].

## RESULTS AND DISCUSSION

### Validation of the Present Model with Analytical Model [36] and Numerical Model [21]

The present model is validated by an analytical model proposed by Kim and Kim [36] and a numerical model presented by Chavan et al. [21] for the growth rate  $\left(\frac{dr}{dt}\right)$  of the droplet as a function of the radius ( $r$ ) of the droplet given in eq (16). The analytical model produces continuous results for different contact angles ( $\theta = 90^\circ, 120^\circ, 150^\circ$  &  $170^\circ$ ) as shown in Figure 2. Whereas, in the numerical model, the discontinuities are noted in Figure 2. due to three different correlations, i)  $Bi < 0.5$  ii)  $0.5 < Bi < 2$ , and iii)  $Bi > 2$ , for predicting the  $Nu$  are used by Chavan et al. [21]

Chavan et al. [21] compared the experimental growth of the droplet with numerical results and Kim's analytical results and reported analytical model underestimates the growth rate due to the lack of taking into account local heat transfer effects at the three-phase contact line. Also, it was observed in the experiments that the large droplet diameters

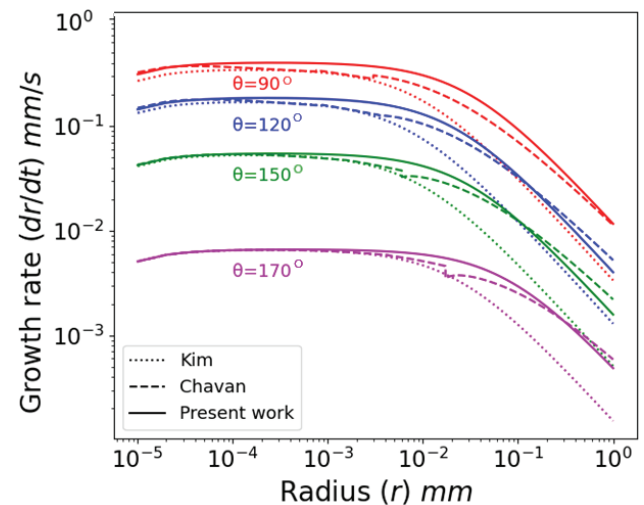


**Figure 2.** Validation of the present model with Kim's analytical model [36] and Chavan's numerical model [21] regarding growth rate.

growing on the superhydrophobic surface lower the growth rates due to added conduction thermal resistance and low droplet diameters growing faster due to interfacial thermal resistance dominated growth [21].

When the contact angle  $\theta = 90^\circ$ , the present model deviates from the numerical model at a radius of the droplet  $r \approx 50 \mu m$  and it produces an identical result at  $r = 1 mm$ . The present model made good agreements with the numerical results when the contact angle increases from  $\theta = 90^\circ$  to  $\theta = 170^\circ$  as shown in Figure 2. Hence, the present model is best suitable for dropwise condensation on hydrophobic and superhydrophobic interfaces.

**Validation of the Present Model with the Experimental works [21,24]**

The present model is also validated by experimental results obtained by Chavan et al. [21] and Enright et al. [24] for the radius of the droplet  $r$  as a function of time  $t$ . The experimental results are shown in Figures 3 (a) and

(b) obtained by Chavan et al. for the subcooling temperature  $\Delta T_{experimental} = 5^\circ C$  and corresponding contact angles  $\theta = 140^\circ$  and  $\theta = 170^\circ$  respectively. In the present work, the  $\Delta T_{numerical} = 0.0545^\circ C$  for  $\theta = 140^\circ$  and  $\Delta T_{numerical} = 0.092^\circ C$  for  $\theta = 170^\circ$  are taken by mapping the experimental results and made an excellent agreement for the case  $\theta = 140^\circ$  and good agreement made for the  $\theta = 170^\circ$ . The difference between the present model and the experiments can be recognized as the presence of noncondensable gases (NCG). Rose reported that the condensation of water vapor in the presence of NCGs (air) acts as a diffusion barrier for water vapor [15].

The present model is also validated by another experimental result obtained by Enright et al. [24] best fits with  $\Delta T_{numerical} = 0.064^\circ C$  as shown in Figure 3 (c). To obtain the complete simulation of the present model by varying contact angles from  $\theta = 90^\circ \rightarrow 180^\circ$ , the  $\Delta T_{numerical} = 0.0545^\circ C$  is used due to its best fit with experimental results.

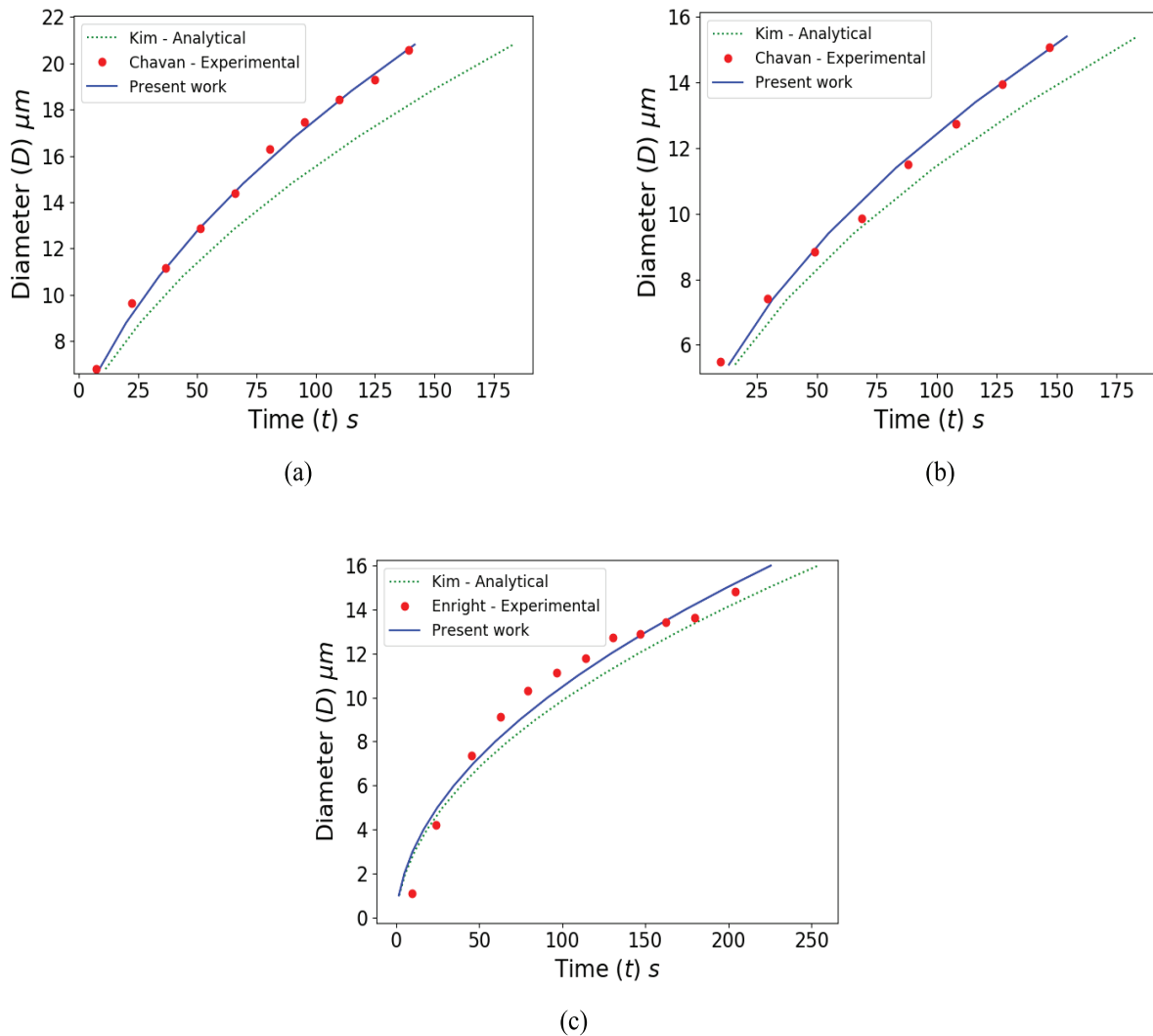


**Figure 3.** Validation of present work with Kim’s analytical [36] and Chavan’s experimental work [21] for (a) contact angle  $\theta = 140^\circ$ , (b) contact angle  $\theta = 170^\circ$  and Enright’s experimental work [24] for (c) contact angle  $\theta = 120^\circ$ .

**Simulation of Heat Transfer Through a Single Droplet**

In the present work, the heat transfer, heat drop, interface temperature variation, and growth rates are analyzed by simulating the eq (14) for different values of Biot number and contact angles. Since the Biot number is a function of the contact angle and radius of the droplet,  $Bi = f(\theta, r)$  the variation of droplet radius is shown in Figure 4. The droplet radius measures the macro scale for the Biot numbers in the range of  $10 > Bi > 1000$ , microscale for the Biot numbers in the range of  $0.01 > Bi > 1$ , and nanoscale for the Biot numbers  $0.00001 > Bi > 0.001$ . Since the minimum thermodynamically viable radius  $r_{min} \approx 10 \text{ nm}$  size, the range of Biot numbers in the present work is chosen from  $Bi = 0.0001 \rightarrow 1000$ . Because of the spherical nature of the droplet, the radius of the droplet varies in a similar pattern against the contact angles  $\theta = 90^\circ$  to  $\theta \approx 180^\circ$  for different Biot numbers, as shown in Figure 4.

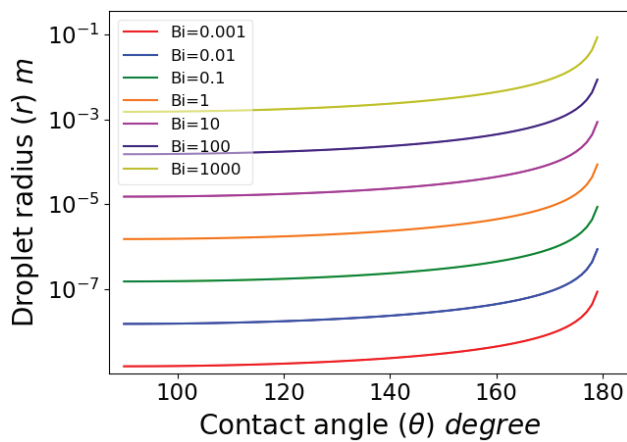


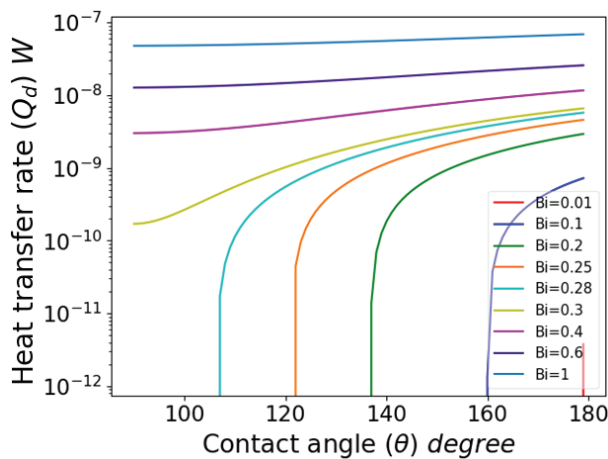
**Figure 4.** Variation of droplet radius with contact angle for different Biot numbers ( $Bi = 0.001 \rightarrow 1000$ ).

The heat transfer through a single droplet  $Q_d$  is shown in Figure 5 for different Biot numbers  $Bi = 0.01 \rightarrow 1$  in Figure 5 (a) and  $Bi = 4 \rightarrow 1000$  in Figure 5 (b). The thermodynamically viable radius of a droplet can be expressed in the form as

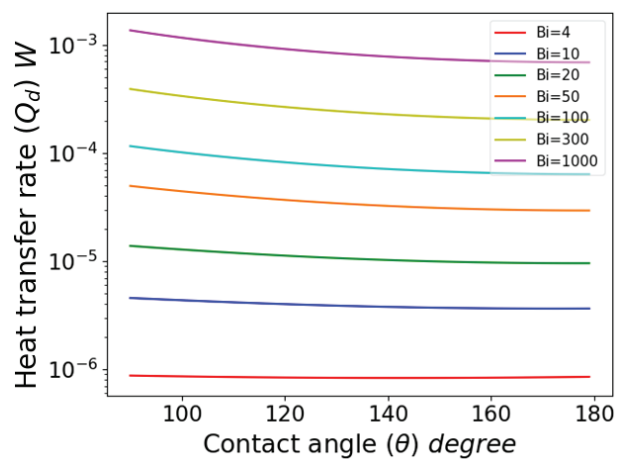
$$r_{min} = \frac{2T_{sat}\sigma}{h_{fg} \rho \Delta T} \tag{17}$$

Where  $\sigma$  is the surface tension of the water, in the literature, the subcooling temperature has been taken in the range  $\Delta T = 1K - 10K$ . The subcooling temperature  $\Delta T = 10K$  and the corresponding minimum viable radius of the droplet  $r_{min} \approx 10 \text{ nm}$  are used to solve the present model [21,34,36]. In the present work, the numerical subcooling temperature is taken as  $\Delta T_{numerical} = 0.0545 \text{ K}$  for the best fit of experimental data and the respective viable radius  $r_{min} \approx 400 \text{ nm}$  is used for simulation. The curvature effect  $1 - \frac{r_{min}}{r}$  is used in eq (14) becomes negative when the radius of the droplet  $r$  is smaller than the  $r_{min}$  value i.e.  $400 \text{ nm}$ . From this point forward, whatever the values are in the negative sign means that  $r < r_{min}$ .

The heat transfer through a single droplet  $Q_d$  is plotted as a function of contact angles varying from  $\theta = 90^\circ \rightarrow 180^\circ$  as shown in Figure 5. When the  $Bi < 0.3$ , the heat transfer through the droplet is very small due to high interface resistance and curvature resistance. The heat transfer rate increases with an increase in contact angle for  $Bi > 0.3$  as shown in Figure 5 (a). Further, with an increase in Biot number towards  $Bi = 1$  the variation of heat transfer follows linearly and approaches a constant line when  $Bi = 4$  as shown in Figure 5 (b). The heat transfer remains constant for all the values of contact angles in both hydrophobic and superhydrophobic sides at  $Bi = 4$ . The heat transfer rate decreases with an increase in contact angle when the Biot number is increased from  $Bi = 4 \rightarrow 1000$  as shown in Figure 5 (b). It is essential to study the variations in the region of  $Bi < 0.3$ , to 1000.



(a)



(b)

**Figure 5.** Heat transfer rate for different contact angles (a)  $Bi = 0.01 \rightarrow 1$  and (b)  $Bi = 4 \rightarrow 1000$ .

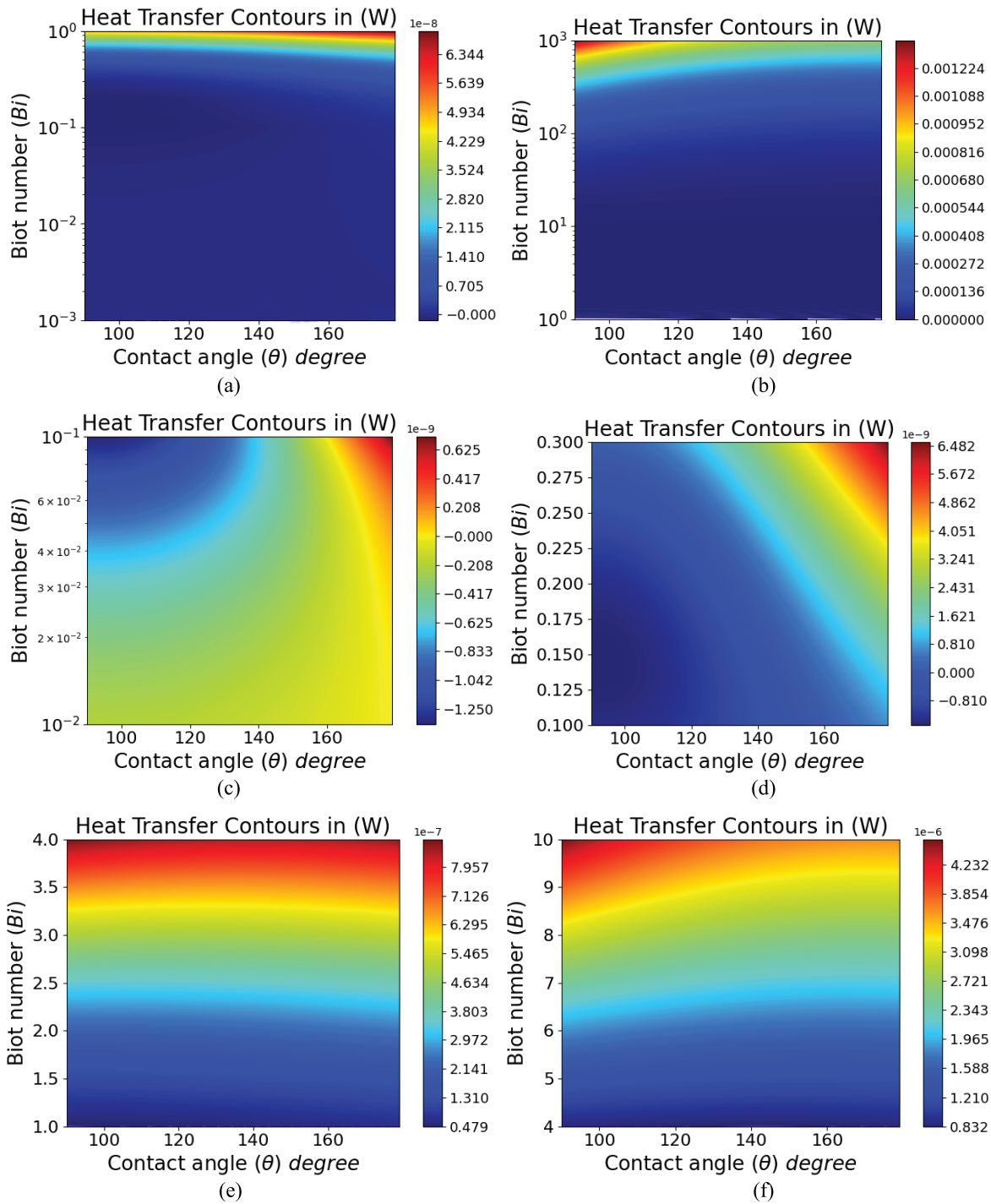


**Figure 6.** Heat transfer contours for different contact angles (a)  $Bi = 0.001 \rightarrow 1$ , (b)  $Bi = 1 \rightarrow 1000$ , (c)  $Bi = 0.01 \rightarrow 1$ , (d)  $Bi = 0.1 \rightarrow 0.3$ , (e)  $Bi = 1 \rightarrow 4$ , and (f)  $Bi = 4 \rightarrow 10$ .

The heat transfer variations from  $Bi = 0.001 \rightarrow 1000$  are predicted by using the modified model eq (14), and contours are plotted as shown in Figure 6 (a-b). The maximum heat transfer rate in the superhydrophobic region for lower Biot numbers shown in Figure 6 (a) is shifted to the hydrophobic region for higher Biot numbers as shown in Figure 6 (b). Figure 6 (c-f) shows the higher

heat transfer shifting behavior for different ranges of Biot numbers  $Bi = 0.01 \rightarrow 0.1$ ,  $Bi = 0.1 \rightarrow 0.3$ ,  $Bi = 1 \rightarrow 4$ , and  $Bi = 4 \rightarrow 10$  respectively. The cold spot (lower heat transfer rate) in the hydrophobic region and the hot spot (higher heat transfer rate) in the superhydrophobic region for  $Bi = 0.01 \rightarrow 0.1$  are shown in Figure 6 (c). The cold spot propagates hydrophobic to the superhydrophobic region,

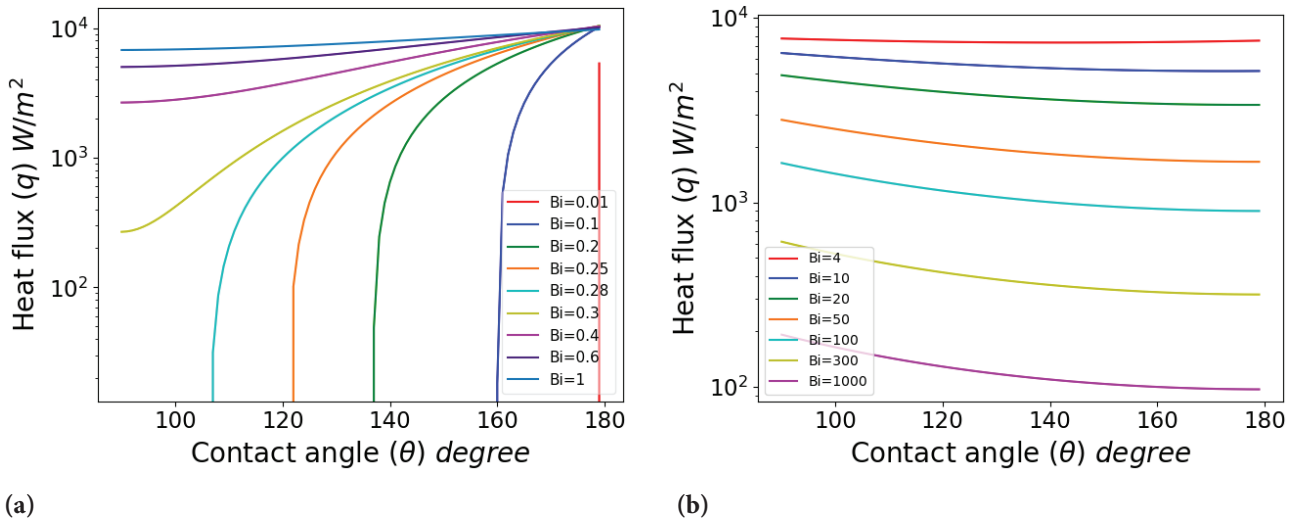


**Figure 7.** Heat flux with different contact angles for (a)  $Bi = 0.01 \rightarrow 1$  and (b)  $Bi = 1 \rightarrow 1000$ .

and  $Bi = 0.1 \rightarrow 0.3$  both regions become cold spots, as shown in Figure 6 (d). An important finding is observed in Figure 6 (e) that the hot spot is almost the same for all contact angles at  $Bi = 4$ . In Figure 6 (f), the hot spot is shifted from the superhydrophobic to the hydrophobic region at  $Bi = 10$  and the heat transfer rate decreases as the contact angle increases.

The heat flux  $q_d$  is the ratio between the heat transfer rate of a single droplet  $Q_d$  and the contact area of the droplet between the solid and liquid interface. Figure 7 (a) shows the heat flux varies nearly similar to the heat transfer rate up to  $Bi = 4$ . In Figure 7 (b), the heat flux is constant throughout the hydrophobic and superhydrophobic region at  $Bi = 4$ , and afterward, increase in Biot number decreases the heat flux due to the high conductive resistance offered by the solid-liquid interface area. When the  $Bi > 4$ , the heat flux decreases for increases in contact angle.

The heat drop due to various resistances, interface resistance  $\Delta T_{Int}$ , curvature resistance  $\Delta T_{Curv}$ , droplet resistance  $\Delta T_{Drop}$ , and coating resistance  $\Delta T_{Coat}$  are analyzed and shown in Figures 8-11 for different Biot numbers. In the condensation process, the first and foremost resistance is interfacial resistance.

Eq (1) is used to predict the heat drop due to interfacial resistance for  $Bi = 0.01 \rightarrow 1$  as shown in Figure 8 (a), the maximum heat drop is attained at  $Bi = 1$ , and for  $Bi = 1 \rightarrow 1000$  as shown in Figure 8 (b), the heat drop decreases when the Biot number increases. For all the Biot numbers, when  $Bi > 0.3$ , minimum heat drop in the superhydrophobic region is occurred due to the large interface area offered by the superhydrophobic surface. When the contact angle exceeds  $170^\circ$ , Figures 8 (a) and (b) show a sudden heat drop. The increase in the contact angle decreases the heat drop due to the greater interfacial resistance offered by the liquid-vapor

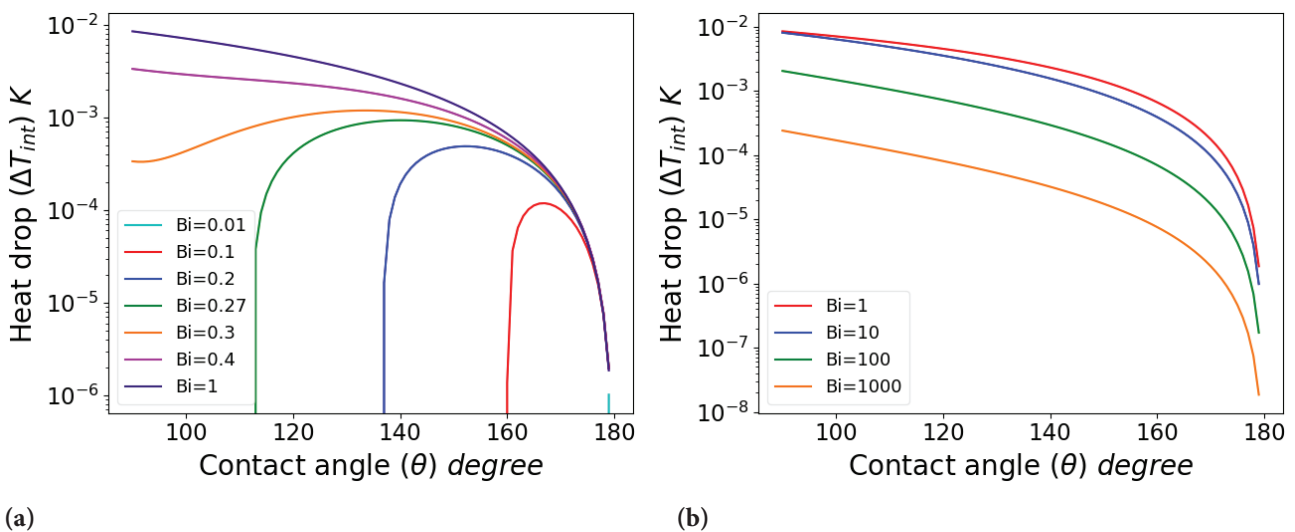


**Figure 8.** Heat drop due to interfacial resistance between droplet and vapor with contact angles ( $\theta = 90^\circ \rightarrow 179^\circ$ ) for different Biot numbers (a)  $Bi = 0.01 \rightarrow 1$  and (b)  $Bi = 1 \rightarrow 1000$ .

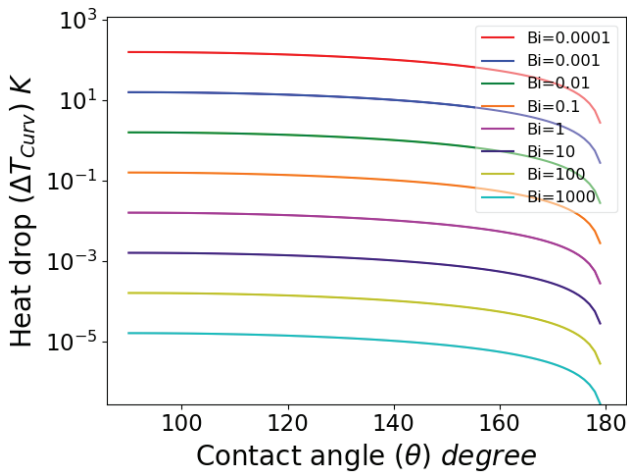


**Figure 9.** Heat drop due to curvature effect with contact angles ( $\theta = 90^\circ \rightarrow 179^\circ$ ) for different Biot numbers ( $Bi = 0.0001 \rightarrow 1000$ ).

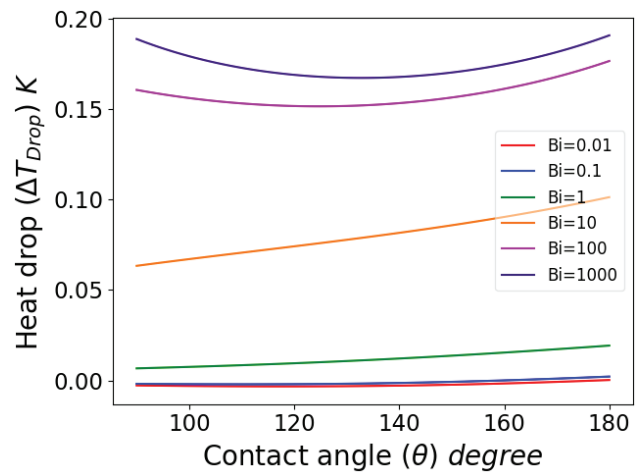


**Figure 10.** Heat drop due to conductive resistance inside the droplet with contact angles ( $\theta = 90^\circ \rightarrow 179^\circ$ ) for different Biot numbers ( $Bi = 0.01 \rightarrow 1000$ ).

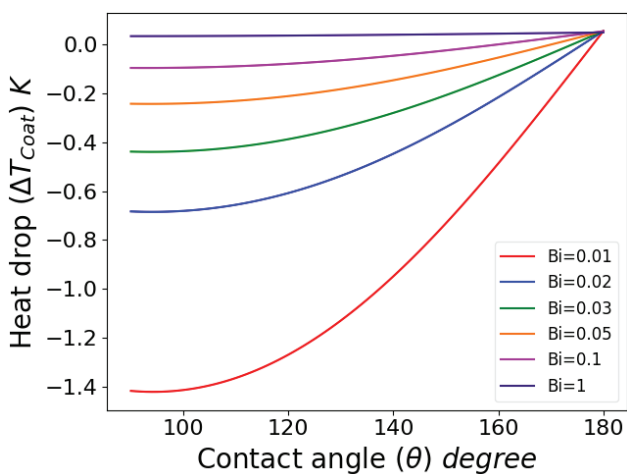
interface. For a lower Biot number, the liquid-vapor surface area approaches zero, resulting in heat drop due to interfacial resistance, as shown in Figure 8 (a). The maximum heat drop of  $\Delta T_{Int} = 0.008 \text{ K}$  is obtained for  $Bi = 1$  and  $\theta = 90^\circ$ , which is 15% of the total heat drop  $\Delta T_{Int} = 0.0545 \text{ K}$ .

The heat drop due to curvature resistance  $\Delta T_{Curv}$  is predicted using the eq (2) for different Biot numbers shown in Figure 9. The curvature resistance only depends on the droplet's radius, and the variation shows an identical pattern for all the Biot numbers. The maximum heat drop in Figure 9 is noted for the lowest Biot number  $Bi = 0.0001$  and decreases with an increase in Biot numbers. For larger values of Biot numbers, the curvature effect can be neglected. The curvature resistance decreases for increases in contact angles, and the maximum heat drop for the  $Bi = 1$  is obtained as  $\Delta T_{Curv} = 0.02$ , which is 37% of the total heat drop.

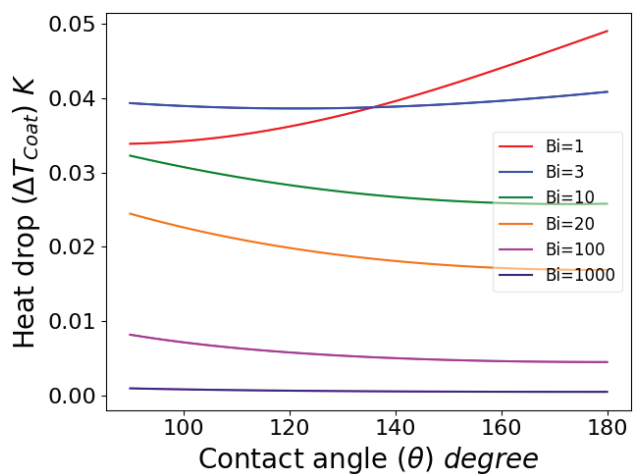
Eq (11) is the modified heat drop  $\Delta T_{Drop}$  due to droplet resistance and predicts the heat drops for different Biot numbers, as shown in Figure 10. The conductive resistance offered by the droplet is the primary source of heat drop for  $Bi > 0.1$ . The heat drop due to conductive resistance increases with an increase in contact angles for the Biot numbers  $Bi = 0.1 \rightarrow 10$  and closely follows linear variation.

When the Biot number is greater than 100, the heat drop decreases in the hydrophobic region from contact angle  $\theta = 90^\circ \rightarrow 140^\circ$  and increases in the superhydrophobic region. The maximum heat drop occurs at a contact angle  $\theta \approx 180^\circ$  for  $Bi = 1$  is  $\Delta T_{Drop} = 0.02 \text{ K}$  and at  $\theta = 90^\circ$   $\Delta T_{Drop} = 0.005 \text{ K}$  which is 9% of the total heat drop.

The coating resistance is predicted by using Eq (4) for different Biot numbers shown in Figures 11 (a) and (b). The



(a)



(b)

**Figure 11.** Heat drop due to coating resistance with contact angles ( $\theta = 90^\circ \rightarrow 179^\circ$ ) for different Biot numbers (a)  $Bi = 0.01 \rightarrow 1$  and (b)  $Bi = 1 \rightarrow 1000$ .

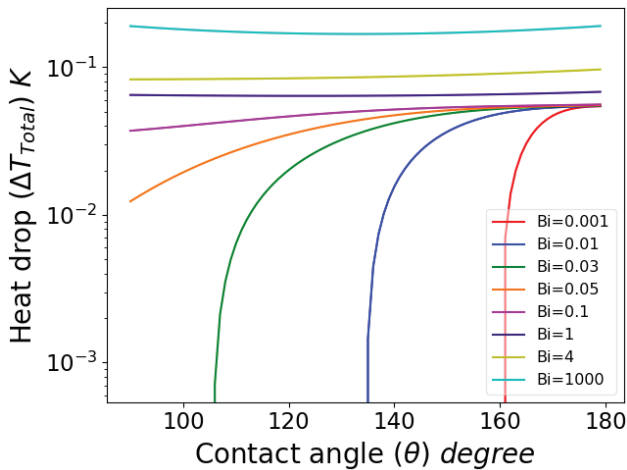


**Figure 12.** Total heat drop through the droplet with contact angles ( $\theta = 90^\circ \rightarrow 179^\circ$ ) for different Biot numbers ( $Bi = 0.001 \rightarrow 1000$ ).

coating thickness  $\delta = 1 \mu\text{m}$  is assumed to predict heat drop due to the coating resistance  $\Delta T_{Coar}$ . Figure 11 (a) shows the heat drop variation for  $Bi = 0.01 \rightarrow 1$  with an increase in contact angle increases in heat drop obtained. At  $Bi = 3$ , the interpretation of heat drop closely follows constantly for all the contact angles in the hydrophobic and superhydrophobic regions, as shown in Figure 11 (b). The contact area of liquid and solid increases when the radius of the droplets increases from micro size to macro size. Since the droplet radius is under micron size for Biot number  $Bi = 1$ , the heat drop due to coating resistance decreases when the Biot number increases greater than one. Further increase in Biot number offers a decrease in heat drop due to coating resistance. When  $Bi > 3$ , the heat drop decrease with an increase in contact angles.

The total heat drop is shown in Figure 12 for the Biot numbers varies from  $Bi = 0.001 \rightarrow 1000$ . The total heat drop  $\Delta T_{Total}$  decreases with an increase in contact angle when the  $Bi < 1$ . There is no variation in the total heat drop for  $Bi = 1$ , and it remains constant for all the contact angles in both the hydrophobic and superhydrophobic regions. The inner resistance to the surface resistances of the droplet is the same at Biot number  $Bi = 1$ . The heat drop increases when the contact angle increases for the  $Bi > 1$ . For more significant value Biot numbers, superhydrophobic regions offer higher total heat drops, as shown in Figure 12.

The Nusselt number, the ratio of conductive resistance to convective resistance, and variation for different Biot numbers are shown in Figure 13. The superhydrophobic interface gives a more prominent value Nusselt number compared with the hydrophobic interface up to  $Bi \approx 5$  with a minimal magnitude due to low conductive resistances than convection. Whereas Biot number  $Bi > 5$ , the shift has occurred, and the hydrophobic interface offers a more

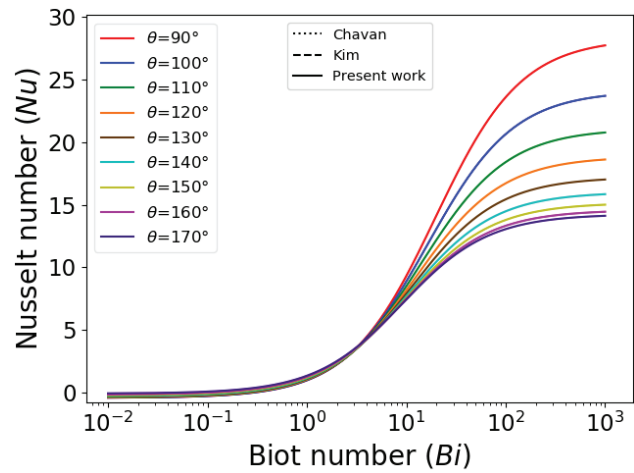


**Figure 13.** Variation of Nusselt number as a function of Biot number ( $Bi = 0.01 \rightarrow 1000$ ) for different contact angles ( $\theta = 90^\circ \rightarrow 170^\circ$ ).

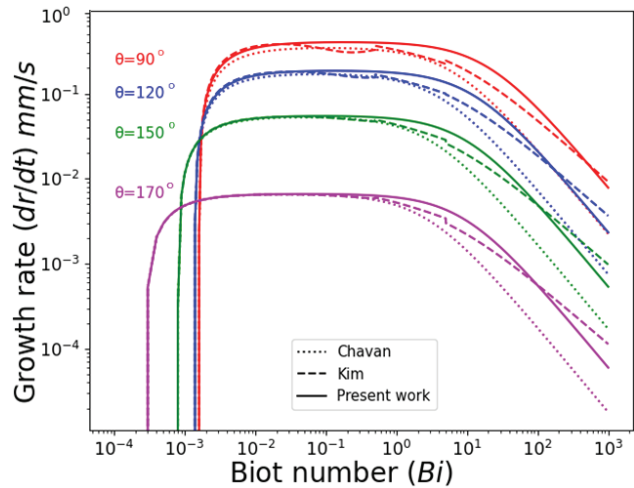


**Figure 14.** Growth rate variation with Biot number ( $Bi = 0.0001 \rightarrow 1000$ ) for different contact angles  $\theta = 90^\circ, 120^\circ, 150^\circ$  &  $170^\circ$ .

considerable value of Nusselt number than the superhydrophobic interface due to higher conductive resistance than the convection.

The growth rate  $dr/dt$  as a function of Biot number  $Bi = 0.0001 \rightarrow 1000$  for different contact angles is shown in Figure 14. For all contact angles, the growth rate remains constant for a specific range of Biot numbers. The content of growth rate increase for superhydrophobic interfaces with lower magnitude and higher growth rate with a comparatively short degree for hydrophobic interfaces are shown in Figure 14 with an accuracy of  $10^{-4}$ .

**Comparison of Hydrophobic and Superhydrophobic Heat Transfer**

In the previous section, the simulation of heat transfer is predicted by using the present modified heat transfer model given by eq (14) which correlates Biot number and contact angle. For complete simulation for the range of contact angle  $\theta = 90^\circ \rightarrow 180^\circ$  and Biot numbers  $Bi = 0.0001 \rightarrow 1000$ , the numerical subcooling temperature

was taken as  $\Delta T_{numerical} = 0.0545$ . The present modified model validated with the experimental work, as shown in Figure 3 (a) and (b) are directly used to compare the heat transfer for the contact angles  $\theta = 140^\circ$  and  $\theta = 170^\circ$ . The numerical subcooling temperature for the contact angle  $\theta = 170^\circ$  is taken as  $\Delta T_{numerical} = 0.092$  for the best fit, as shown in Figure 3 (b). The crucial findings are noted for different resistances, and Nusselt number variations are

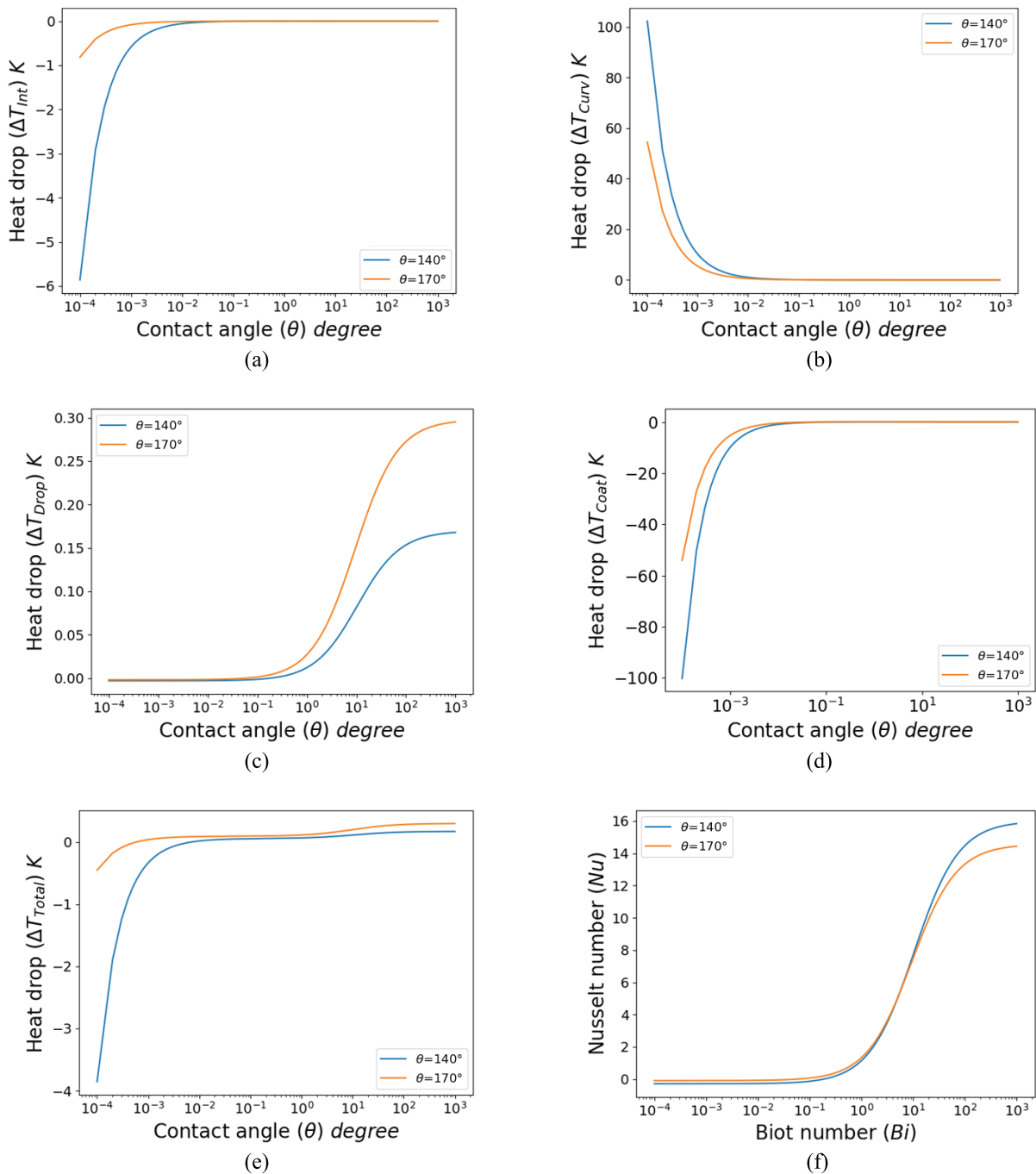


**Figure 15.** Comparison of hydrophobic ( $\theta = 140^\circ$ ) and superhydrophobic ( $\theta = 170^\circ$ ) heat transfer for different Biot numbers ( $Bi = 0.0001 \rightarrow 1000$ ) (a) interfacial heat drop (b) curvature heat drop, (c) droplet heat drop, (d) coating heat drop, (e) total heat drop and (f) Nusselt number.

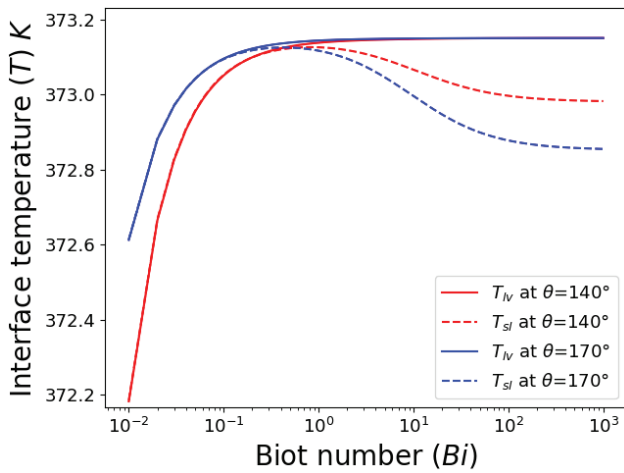


**Figure 16.** Interface temperature as a function of the Biot number for different contact angles ( $\theta = 140^\circ$  &  $170^\circ$ ).

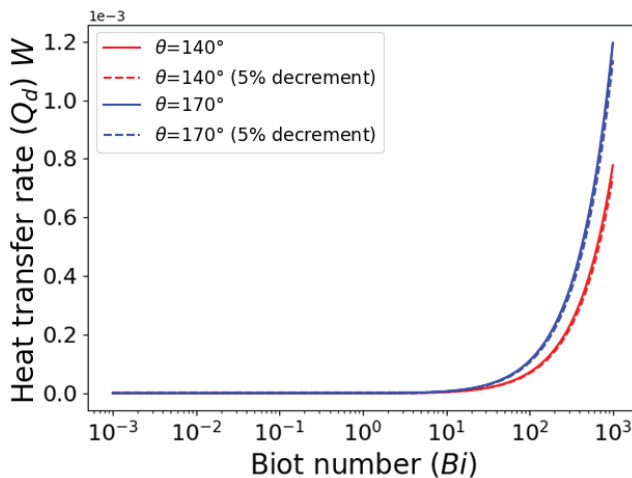
shown in Figure 15 (a-f). The interfacial resistance affects the heat drop intensively when the Biot number  $Bi < 0.1$  due to low conductive resistance and remains constant for both contact angles, as shown in Figure 15 (a). The curvature effect is significant for the Biot number  $Bi < 0.04$  and remains constant, as shown in Figure 15 (b). The vital finding observed in Figure 15 (c) is that a massive heat drop occurred in the range of Biot numbers  $Bi = 1 \rightarrow 100$  due to higher heat transfer through the droplet by conduction. The heat drop due to conduction for the superhydrophobic interface is higher than for the hydrophobic interface. When the  $Bi < 0.01$ , the heat transfer through the droplet is negligible, and most of the heat drop is carried by the curvature effect and interface resistance. The coating resistance is also significant for the Biot number

$Bi < 0.05$ , as shown in Figure 15 (d). For Biot number in the range  $Bi = 0.01 \rightarrow 1$ , the total heat drop produces a marginal difference, significant variation for Biot number  $Bi < 0.01$ , and a moderate difference is noted for higher Biot numbers as shown in Figure 15 (e). Figure 15 (f) shows the variation of the Nusselt number as a function of the Biot number in which the variation is shifted at  $Bi \approx 5$ , and the Nusselt number decreases for higher contact angles.

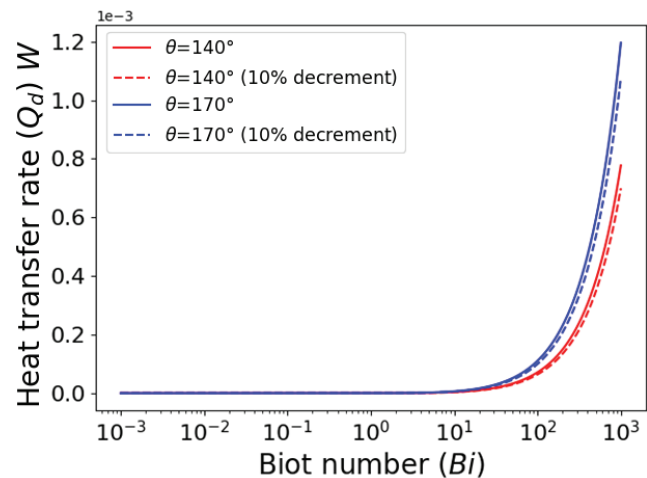
The interface temperatures, liquid-vapor interface, and solid-liquid are also predicted by using the Eqns (1, 2, 4, 11) for the contact angles  $\theta = 140^\circ$  and  $\theta = 170^\circ$ . The liquid-vapor interface temperatures  $T_{lv}$  decreases immensely for the Biot number  $Bi < 2$  due to a large amount of heat transfer through tiny droplets and remains unchanged for the higher value of Biot numbers due to higher conductive resistance offered by the droplets. The maximum interface temperature  $T_{lv}$  is obtained at Biot number  $Bi > 2$  for both contact angles  $\theta = 140^\circ$  and  $\theta = 170^\circ$ . The solid-liquid interface temperature  $T_{sl}$  exactly follows its variation up to  $Bi \approx 0.4$  for  $\theta = 140^\circ$  and  $Bi \approx 0.2$  for  $\theta = 170^\circ$ , as shown in Figure 16. The maximum interface temperature  $T_{sl}$  for the contact angle,  $\theta = 140^\circ$  and  $\theta = 170^\circ$  are obtained at  $Bi \approx 0.5$  and  $Bi \approx 0.4$  respectively. The interface temperature  $T_{sl}$  decreases for the higher values of Biot number.

**Heat Transfer Rate Variation with Model Sensitivity**

The present model sensitivity is observed by changing the subcooling temperature  $\Delta T$  and minimum viable radius  $r_{min}$ . Figure 17 (a) and (b) show that the heat transfer rate variation for different Biot numbers varies from  $Bi = 0.001 \rightarrow 1000$  by changing  $\Delta T$  and  $r_{min}$  by 5% and 10% respectively. The present model is low sensitive for lower size droplets of radius  $r < 10 \mu m$  and slightly higher sensitive for larger droplets of radius  $r > 10 \mu m$  as shown in Figure 17 (a). At  $Bi$



(a)



(b)

**Figure 17.** Heat transfer rate variation with model sensitivity by changing  $\Delta T$  &  $r_{min}$  by (a) 5% decrement and (b) 10% decrement.

= 10, the hydrophobic interface produces a 4% reduced heat transfer rate, and the superhydrophobic interface makes a 5% reduced heat transfer rate for a 5% decrement in the values of  $\Delta T$  and  $r_{min}$ . At  $Bi = 1000$ , the maximum reduction of 6% heat transfer obtained in the superhydrophobic interface and hydrophobic interface provides a 5% reduction in heat transfer. Whereas for a 10% decrement, the maximum reduction in heat transfer of 11% is obtained from the superhydrophobic interface at Biot number  $Bi = 1000$  as shown in Figure 17 (b).

## CONCLUSION

An unique heat transfer model for dropwise condensation on the hydrophobic and superhydrophobic interface is developed by correlating the Biot number and contact angle. The developed model is validated with analytical, numerical, and experimental work, offering excellent agreement. The present heat transfer model is modified for the best fit of observed values. The modified heat transfer model is used to predict the heat transfer through the single droplet, heat flux, heat drops due to various resistances such as interfacial resistance, curvature resistance, droplet resistance, coating resistance, the growth rate of the droplet, and interfacial temperatures for different Biot numbers varies from  $Bi = 0.0001 \rightarrow 1000$  and different contact angles in the range  $\theta = 90^\circ \rightarrow 180^\circ$ . Besides, heat transfer contours are plotted for other Biot numbers as a function of contact angles. From the simulation of the present modified model, the following are the findings for dropwise condensation on hydrophobic and superhydrophobic interfaces,

- A continuous single correlation model predicts the heat transfer for a vast range of Biot numbers  $Bi = 0.0001 \rightarrow 1000$
- For the best fit, the numerical value for subcooling temperature is found as  $\Delta T_{numerical} = 0.0545 K$  against the experimental value  $\Delta T_{experimental} = 5 K$ .
- At  $Bi = 4$ , the heat transfer rate remains unchanged for all the contact angles in the hydrophobic and superhydrophobic regions.
- A wide variation of the growth rate for all the Biot numbers in the range  $Bi = 0.0001 \rightarrow 1000$  is presented.
- The heat drop due to interfacial resistance reaches a maximum value at  $Bi = 1$ .
- For  $Bi = 1$ , the total heat drops are almost constant for all the contact angles in the hydrophobic and superhydrophobic regions.
- The Nusselt number shift occurs at  $Bi \approx 5$ .
- The interfacial resistance and curvature effect, and coating resistance are significant for  $Bi < 0.01$ , and droplet resistance is substantial for  $Bi > 0.05$ .
- The liquid-vapor interface temperature reaches its maximum value at  $Bi \approx 5$  and remains constant afterward.
- The solid-liquid interface temperature reaches a maximum at  $Bi \approx 0.4 \rightarrow 0.5$  and decreases afterward.

## NOMENCLATURE

$Bi$	Biot number
$Nu$	Nusselt number
$\theta$	Contact angle, degree
$r$	Droplet radius, m
$r_{min}$	Minimum viable radius, m
$r_{max}$	Maximum radius, m
$Q$	Heat transfer rate, W
$\Delta T$	Temperature difference, K
$h_i$	Interface heat transfer coefficient, W/m <sup>2</sup> K
$\delta$	Coating thickness, m
$k$	Thermal conductivity, W/mK
$\rho$	Density, kg/m <sup>3</sup>
$h_{fg}$	Latent heat, J/kg
$dr/dt$	Growth rate, m/s
$r_c$	Contact radius, m
$h$	Droplet height, m
$V$	Volume, m <sup>3</sup>
$H$	Effective height, m
$a$ & $b$	Empirical value
$c$	Condensation coefficient

## REFERENCES

- [1] McNeil DA, Burnside BM, Cuthbertson G. Dropwise condensation of steam on a small tube bundle at turbine condenser conditions. *Exp Heat Transf* 2000;13:89–105. [CrossRef]
- [2] Kurshakov AV, Ryzhenkov AV, Bodrov AA, Ryzhenkov OV, Patakin AA, Chernov EF. Heat transfer enhancement in steam-turbine condensers with the use of surface-active substances. *Therm Eng* 2014;61:785–789. [CrossRef]
- [3] Beér JM. High efficiency electric power generation: The environmental role. *Prog Energy Combust Sci* 2007;33:107–134. [CrossRef]
- [4] Lara JR, Noyes G, Holtzapple MT. An investigation of high operating temperatures in mechanical vapor-compression desalination. *Desalination* 2008;227:217–232. [CrossRef]
- [5] Peters TB, McCarthy M, Allison J, Dominguez-Espinosa FA, Jenicek D, Kariya HA, et al. Design of an integrated loop heat pipe air-cooled heat exchanger for high performance electronics. *IEEE Trans Components Packag Manuf Technol* 2012;2:1637–1648. [CrossRef]
- [6] Kim MH, Bullard CW. Air-side performance of brazed aluminum heat exchangers under dehumidifying conditions. *Int J Refrig* 2002;25:924–934. [CrossRef]
- [7] Li B, Yao R. Urbanisation and its impact on building energy consumption and efficiency in China. *Renew Energy* 2009;34:1994–1998. [CrossRef]
- [8] Pérez-Lombard L, Ortiz J, Pout C. A review on buildings energy consumption information. *Energy Build* 2008;40:394–398. [CrossRef]

- [9] Sett S, Sokalski P, Boyina K, Li L, Rabbi KF, Auby H, et al. Stable Dropwise Condensation of Ethanol and Hexane on Rationally Designed Ultrascaleable Nanostructured Lubricant-Infused Surfaces. *Nano Lett* 2019;19:5287–5296. [CrossRef]
- [10] Schmidt E, Schurig W, Sellschopp W. Versuche über die Kondensation von Wasserdampf in Film- und Tropfenform. *Techn Mech Thermodyn* 1930;1:53–63. [Deutsch] [CrossRef]
- [11] Le Fevre EJ, Rose JW. An experimental study of heat transfer by dropwise condensation. *Int J Heat Mass Transf* 1965;8:1117–1133. [CrossRef]
- [12] Rose JW. On the mechanism of dropwise condensation. *Int J Heat Mass Transf* 1967;10:755–762. [CrossRef]
- [13] Stylianou SA, Rose JW. Drop-to-filmwise condensation transition: Heat transfer measurements for ethanediol. *Int J Heat Mass Transf* 1983;26:747–760. [CrossRef]
- [14] Burnside BM, Hadi HA. Digital computer simulation of dropwise condensation from equilibrium droplet to detectable size. *Int J Heat Mass Transf* 1999;42:3137–3146. [CrossRef]
- [15] Rose JW. Dropwise condensation theory and experiment: A review. *Proc Inst Mech Eng Part A J Power Energy*. 2002;216:115–128. [CrossRef]
- [16] Vemuri S, Kim KJ. An experimental and theoretical study on the concept of dropwise condensation. *Int J Heat Mass Transf* 2006;49:649–657. [CrossRef]
- [17] Leach RN, Stevens F, Langford SC, Dickinson JT. Dropwise condensation: Experiments and simulations of nucleation and growth of water drops in a cooling system. *Langmuir* 2006;22:8864–8872. [CrossRef]
- [18] Zhong L, Xuehu M, Sifang W, Mingzhe W, Xiaonan L. Effects of surface free energy and nanostructures on dropwise condensation. *Chem Eng J* 2010;156:546–552. [CrossRef]
- [19] Miljkovic N, Enright R, Wang EN. Effect of droplet morphology on growth dynamics and heat transfer during condensation on superhydrophobic nanostructured surfaces. *ACS Nano* 2012;6:1776–1785. [CrossRef]
- [20] Peng B, Ma X, Lan Z, Xu W, Wen R. Experimental investigation on steam condensation heat transfer enhancement with vertically patterned hydrophobic-hydrophilic hybrid surfaces. *Int J Heat Mass Transf* 2015;83:27–38. [CrossRef]
- [21] Chavan S, Cha H, Orejon D, Nawaz K, Singla N, Yeung YF, et al. Heat transfer through a condensate droplet on hydrophobic and nanostructured superhydrophobic surfaces. *Langmuir* 2016;32:7774–7787. [CrossRef]
- [22] Macner AM, Daniel S, Steen PH. Simulating heat transfer during transient dropwise condensation on a low-thermal-conductivity substrate. *Langmuir* 2019;35:11566–11578. [CrossRef]
- [23] Enright R, Miljkovic N, Al-Obeidi A, Thompson CV, Wang EN. Condensation on superhydrophobic surfaces: the role of local energy barriers and structure length scale. *Langmuir* 2012;28:14424–14432. [CrossRef]
- [24] Enright R, Miljkovic N, Dou N, Nam Y, Wang EN. Condensation on superhydrophobic copper oxide nanostructures. *Proceedings of the ASME 2012 Third International Conference on Micro/Nanoscale Heat and Mass Transfer* 2013:135. [CrossRef]
- [25] Ölçeroğlu E, Hsieh CY, Rahman MM, Lau KKS, McCarthy M. Full-field dynamic characterization of superhydrophobic condensation on bio-templated nanostructured surfaces. *Langmuir* 2014;30:7556–7566. [CrossRef]
- [26] Li G, Alhosani MH, Yuan S, Liu H, Ghaferi AA, Zhang T. Microscopic droplet formation and energy transport analysis of condensation on scalable superhydrophobic nanostructured copper oxide surfaces. *Langmuir* 2014;30:14498–14511. [CrossRef]
- [27] Baba S, Sawada K, Tanaka K, Okamoto A. Dropwise condensation on a hierarchical nanopillar structured surface. *Langmuir* 2020;36:10033–10042. [CrossRef]
- [28] Cha H, Vahabi H, Wu A, Chavan S, Kim MK, Sett S, et al. Dropwise condensation on solid hydrophilic surfaces. *Sci Adv* 2020;6:eaax0746. [CrossRef]
- [29] Song Z, Lu M, Chen X. Investigation of dropwise condensation heat transfer on laser-ablated superhydrophobic/hydrophilic hybrid copper surfaces. *ACS Omega* 2020;5:23588–23595. [CrossRef]
- [30] Wang R, Wu F, Xing D, Yu F, Gao X. Density maximization of one-step electrodeposited copper nanocones and dropwise condensation heat-transfer performance evaluation. *ACS Appl Mater Interfaces* 2020;12:24512–24520. [CrossRef]
- [31] Ludwicki JM, Robinson FL, Steen PH. Switchable wettability for condensation heat transfer. *ACS Appl Mater Interfaces* 2020;12:22115–22119. [CrossRef]
- [32] Orazzo A, Tanguy S. Direct numerical simulations of droplet condensation. *Int J Heat Mass Transf* 2019;129:432–448. [CrossRef]
- [33] Stevens KA, Crockett J, Maynes D, Iverson BD. Simulation of drop-size distribution during dropwise and jumping drop condensation on a vertical surface: implications for heat transfer modeling. *Langmuir* 2019;35:12858–12875. [CrossRef]
- [34] Birbarah P, Chavan S, Miljkovic N. Numerical simulation of jumping droplet condensation. *Langmuir* 2019;35:10309–10321. [CrossRef]
- [35] Adhikari S, Nabil M, Rattner AS. Condensation heat transfer in a sessile droplet at varying Biot number and contact angle. *Int J Heat Mass Transf* 2017;115:926–931. [CrossRef]
- [36] Kim S, Kim KJ. Dropwise condensation modeling suitable for superhydrophobic surfaces. *J Heat Transf* 2011;133:081502. [CrossRef]

- [37] Miljkovic N, Enright R, Wang EN. Modeling and Optimization of Superhydrophobic Condensation. *J Heat Transf* 2013;135:111004. [CrossRef]
- [38] Tanasawa I. Advances in Condensation Heat Transfer. In: Hartnett JP, Irvine TF, Cho YI (editors). *Advances in Heat Transfer*. Amsterdam: Elsevier.;1991. Vol. 21, p. 55–139. [CrossRef]
- [39] Glicksman LR, Hunt AW. Numerical simulation of dropwise condensation. *Int J Heat Mass Transf* 1972;15:2251–2269. [CrossRef]
- [40] Graham C, Griffith P. Drop size distributions and heat transfer in dropwise condensation. *Int J Heat Mass Transf* 1973;16:337–346. [CrossRef]
- [41] Sadhal SS, Martin WW. Heat transfer through drop condensate using differential inequalities. *Int J Heat Mass Transf* 1977;20:1401–1407. [CrossRef]
- [42] Yuvaraj R, Senthil Kumar D. Study of droplet dynamics and condensation heat transfer on superhydrophobic copper surface. *Therm Sci* 2021;25:653–664. [CrossRef]
- [43] Wolfram MathWorld. Archimedes' Hat-Box Theorem. Available at: <https://mathworld.wolfram.com/ArchimedesHat-BoxTheorem.html> Last Accessed Date: 26.09.2023.
- [44] Rose JW, Glicksman LR. Dropwise condensation-The distribution of drop sizes. *Int J Heat Mass Transf* 1973;16:411–425. [CrossRef]
- [45] Tanaka H, Tsuruta T. A microscopic study of dropwise condensation. *Int J Heat Mass Transf* 1984;27:327–335. [CrossRef]
- [46] Xu Z, Zhang L, Wilke K, Wang EN. Multiscale dynamic growth and energy transport of droplets during condensation. *Langmuir* 2018;34:9085–9095. [CrossRef]